IEEE Access
Multidisciplinary | Rapid Review | Open Access Journal

Received August 17, 2018, accepted September 11, 2018, date of publication October 12, 2018, date of current version November 8, 2018.

Digital Object Identifier 10.1109/ACCESS.2018.2875737

Spectrogram-Based Non-Contact RRI Estimation by Accurate Peak Detection Algorithm

KOHEI YAMAMOTO[1], (Student Member, IEEE), KENTAROH TOYODA[2], (Member, IEEE), AND TOMOAKI OHTSUKI[2], (Senior Member, IEEE)

[1]Graduate School of Science and Technology, Keio University, Kanagawa 223-8522, Japan
[2]Department of Information and Computer Science, Keio University, Kanagawa 223-8522, Japan

Corresponding author: Tomoaki Ohtsuki (ohtsuki@ics.keio.ac.jp)

ABSTRACT Demands for vital sign monitoring are increasing in the field of health care. In particular, the R-R Interval (RRI) estimation has been studied extensively, since the RRI variation is highly related with the stress of a subject. Various Doppler sensor-based-heartbeat detection methods have been proposed so far, thanks to non-contact and non-invasive features of a Doppler sensor. In our previous research, we have proposed a Doppler sensor-based RRI estimation method by a spectrogram. In this method, the spectra due to heartbeats are integrated on a spectrogram, and then the RRI is estimated by detecting the peaks of the integrated spectrum. However, the undesired peaks sometimes appear even in the situation where a subject sits still. In this paper, as the extended version of our previous method, we propose a Doppler sensor-based RRI estimation method leveraging the accurate peak detection. In the proposed method, to prevent the incorrect peak detection, the peaks due to heartbeats are detected using some peaks before and after the investigated peak. Through the experiments on 10 subjects in the cases where a subject was sitting still, typing, and speaking, we confirmed that the proposed method improved our previous and state-of-the-art ones by the root-mean-squared error of the RRI. Furthermore, based on the estimated RRI, we calculated the stress index low-frequency/high-frequency (LF/HF), which is one of the useful indices to evaluate the stress of a subject. As a result, our proposed method outperformed the other ones by the relative error of the LF/HF.

INDEX TERMS Microwaves, Doppler sensor, spectrogram, health care, heartbeat, RRI (R-R Interval).

I. INTRODUCTION

Vital sign monitoring is receiving a lot of attention in the field of health care. In particular, the heartbeat detection technique has been developed for many years. Thanks to heartbeat detection technique, the variation of the RRI (R-R Interval) can be measured, where the RRI denotes the peak-to-peak interval of heartbeats. The stress index can be calculated based on the spectrum analysis of the RRI variation [1]–[4]. In particular, the LF/HF (Low-Frequency/High-Frequency) assessment is widely used as one of the useful methods to estimate the balance between the sympathetic nervous and the parasympathetic nervous [3], [4].

To measure the stress level through the LF/HF assessment, the Doppler sensor-based heartbeat detection has been studied extensively [5]–[22]. A Doppler sensor can observe the velocity and direction of a moving target by transmitting microwaves toward the target and then analyzing a reflected Doppler-shifted microwaves. Therefore, the Doppler sensor-based heartbeat detection method does not require the device attachment, unlike the method using ECG (Electrocardiograph) and PPG (Photoplethysmogram). In addition, one of its important features is that the transmitted microwaves penetrate the subject's clothes, meaning that the Doppler sensor-based method does not require to take off subject's clothes. However, the accurate heartbeat detection is challenging, because the SNR (Signal-to-Noise Ratio) of heartbeat components over a reflected signal of a Doppler sensor is low, compared with those of respiration and body movements. In general, the chest displacement due to heartbeats ranges from 0.2 mm to 0.5 mm, while that due to respiration ranges from 4 mm to 12 mm [13]. Also, the displacement due to body movements might be larger than those due to respiration and heartbeats, and such body movements might significantly degrade the accuracy of the heartbeat detection. To extract the heartbeat components from the signal

2169-3536 © 2018 IEEE. Translations and content mining are permitted for academic research only.
Personal use is also permitted, but republication/redistribution requires IEEE permission.
See http://www.ieee.org/publications_standards/publications/rights/index.html for more information.

including not only heartbeat components but also non-heartbeat components, e.g., respiration and body movements, various Doppler sensor-based heartbeat detection methods have been proposed so far [5]–[22].

These can be classified into two methods in terms of the way to estimate the RRI: (i) the indirect [5]–[14] and (ii) the direct RRI estimation method [15]–[22]. In the indirect RRI estimation methods, the HR (Heart Rate) is firstly estimated and the RRI is then calculated based on the estimated HR. In contrast, the direct RRI estimation methods estimate the RRI without the HR estimation by extracting each heartbeat component from the received signal of a Doppler sensor. As one of the direct RRI estimation methods, we have previously proposed the one based on a spectrogram [23]. Our previous method integrates the spectra corresponding to heartbeats over a spectrogram, and then estimates the RRI by detecting peaks of the integrated spectrum. However, the undesired peaks sometimes appear around the peaks due to heartbeats. This is mainly because of body movement, and such undesired peaks may result in the incorrect peak detection. In particular, more undesired peaks appear in the situation where a subject moves. Therefore, the peak detection method needs to be improved.

In this paper, as the extended version of our previous method [23], we propose a Doppler sensor-based RRI estimation method leveraging an accurate peak detection method. Unlike our previous method, the peaks due to heartbeats are detected based on some peaks before and after the investigated peak. More specifically, RRI candidates are generated based on the peaks within a time window and then the peaks are detected so that the difference between the generated RRIs and the previously estimated RRI becomes the smallest. Note that the time window used in the peak detection is unlike the widow used in STFT. The time window length is set based on the previously estimated RRI, which means the window length varies over time.

To evaluate the performance of the proposed method, we conducted the experiments on 10 subjects in three cases where a subject was (i) sitting still, (ii) typing, and (iii) speaking. We compared the RRI estimation accuracy of our proposed method with those of our previous and state-of-the-art methods. The experimental results showed that the proposed method significantly outperformed the state-of-the-art ones, and improved the RMSEs of our previous one by 48.8 %, 42.7 %, and 39.1 % in the cases of the sitting still, typing, and speaking, respectively. Furthermore, we calculated the stress index LF/HF based on the estimated RRI, and then we confirmed that our proposed method achieved the lower RE (Relative Error) than our previous and state-of-the-art ones did in all the cases.

The rest of this paper is organized as follows. In Section II, we describe the principle of a Doppler sensor and related work. In Sections III, we explain our proposed method. We then describe the conducted experiments and evaluate the performance of our method in Section IV. Finally, we conclude this paper in Section V.

II. PRELIMINARIES

In this section, we firstly describe the principle of a Doppler sensor. We then explain the related work and the RRI-based stress evaluation method.

A. THE PRINCIPLE OF A DOPPLER SENSOR

Fig. 1 shows the system model of the Doppler sensor-based heartbeat detection. In this system, microwaves $T(t) = \cos\left(2\pi ft + \Phi(t)\right)$ are transmitted from the transmitter Tx towards the subject's chest, where f and $\Phi(t)$ are the carrier frequency and the phase noise, respectively. The transmitted microwaves reflected by the subject's chest are then received by the receiver Rx, where the received signal $R(t)$ is represented as eq. (1).

$$R(t) = \cos\left(2\pi ft - \frac{4\pi d_0}{\lambda} - \frac{4\pi x(t)}{\lambda} + \Phi\left(t - \frac{2d_0}{c}\right)\right), \quad (1)$$

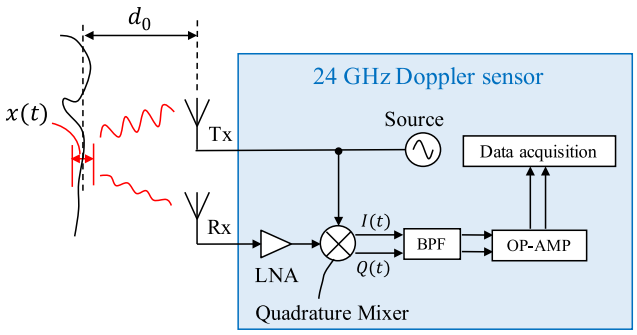

FIGURE 1. The system model of the Doppler sensor-based heartbeat detection.

where c is the speed of the electro-magnetic wave, λ is the wavelength of the carrier and $x(t)$ is the variation of the distance d_0 between a Doppler sensor and the subject's chest. The received signal $R(t)$ is down-converted into the baseband signal $B(t)$.

$$B(t) = \cos\left(\theta + \frac{4\pi x(t)}{\lambda} + \Delta\Phi(t)\right), \quad (2)$$

where θ is the constant phase shift determined by d_0 and f, and $\Delta\Phi(t)$ is the total residual phase noise including the noise accumulated in the circuit and along the transmission path. By applying a quadrature mixer to $B(t)$, the phase of $B(t)$ is shifted by $\pi/2$, which results in two components with a phase difference of $\pi/2$, $I(t)$ and $Q(t)$. The obtained components $I(t)$ and $Q(t)$ are called in-phase and quadrature components, respectively. These are expressed as follows.

$$I(t) = \cos\left(\theta + \frac{\pi}{4} + \frac{4\pi x(t)}{\lambda} + \Delta\Phi(t)\right), \quad (3)$$

$$Q(t) = \cos\left(\theta - \frac{\pi}{4} + \frac{4\pi x(t)}{\lambda} + \Delta\Phi(t)\right). \quad (4)$$

Subsequently, to eliminate the undesired frequency components, BPF (Band Pass Filter) is applied to $I(t)$ and $Q(t)$ signals. The levels of $I(t)$ and $Q(t)$ signals are amplified by

OP-AMP (Operational Amplifier). Finally, a Doppler signal $S(t)$ is calculated using $I(t)$ and $Q(t)$ as eq. (5).

$$S(t) = I(t) + jQ(t). \tag{5}$$

$S(t)$ can be also expressed as follows.

$$\begin{aligned} S(t) &= I(t) + jQ(t), \\ &= \exp\{j[\mp\frac{4\pi vt}{\lambda} + \Phi(t)]\}, \end{aligned} \tag{6}$$

where v is the motion speed of a target. In this equation, the minus and the plus symbols mean the motion direction of a target. When a target moves away from a Doppler sensor, the minus symbol is adapted, and vice versa. The amount of the frequency shift due to a target motion, f_{shift}, is given as

$$f_{shift} = \frac{4\pi vt}{\lambda} \times \frac{1}{2\pi t} = \frac{2v}{\lambda}. \tag{7}$$

B. RELATED WORK

In terms of the way to estimate the RRI, the Doppler sensor-based RRI estimation methods can be classified into two methods: (i) the indirect [5]–[14] and (ii) the direct RRI estimation methods [15]–[22]. In the indirect RRI estimation methods, the HR (Heart Rate) is firstly estimated and the RRI are then calculated based on the estimated HR. The conventional methods estimate the HR leveraging the time-frequency analysis, e.g. (i) FFT (Fast Fourier Transform) [5]–[8], (ii) MUSIC (MUltiple SIgnal Classification) [9], [10], and (ii) WT (Wavelet Transform) [11]–[14]. In general, the normal respiration rate varies between 0.1 Hz and 0.3 Hz [13], while the normal HR does between 0.5 Hz and 2 Hz [24]. Therefore, by applying FFT to the received signal of a Doppler sensor, it is possible to extract the frequency components from the received signal including the respiration components [5]–[8]. Also, to accurately estimate the HR over the received signal including the noise due to not only respiration, but also body movements, the MUSIC-based HR estimation methods have been investigated so far [9], [10]. MUSIC is an algorithm widely used in the field of the DOA (Direction of Arrival) estimation and the frequency estimation. The MUSIC-based method has been shown to be accurate compared with the FFT-based one [9], [10]. However, both the FFT-based and the MUSIC-based HR estimation methods require a time window that includes some heartbeats. In particular, most of such methods use time windows longer than 10 s to achieve a high frequency resolution [5]–[7]. The HR varies within a time window, meaning that the RRI does as well. Therefore, for the achievement of the accurate stress evaluation, it is necessary to analyze the received signal of a Doppler sensor with a higher time resolution. To realize this, the WT-based HR estimation methods have been proposed [11]–[14]. WT is a tool to analyze a signal with a higher time-frequency resolution than FFT (Fast Fourier Transform) by using the prototype signal called mother wavelet. In WT, the frequency of the analyzed signal can be estimated by scaling and shifting the prototype signal. There exist many choices of the prototype signal, and a suitable selection of the prototype signal results in the high accuracy of HR estimation. In related work [11], [12], the HR is estimated by detecting the peak due to heartbeats over the spectrum calculated based on the selected suitable prototype signal. Sekine and Maeno [13] has proposed the HR estimation method based on the periodicity analysis of the time-domain signal obtained through WT. Also, Li and Lin [14] has proposed the fast HR estimation method with a short time window, i.e., from 3 s to 5 s. Through the experiments against a sitting still subject, these methods have been shown to perform the accurate HR estimation, compared with the FFT-based methods [11]–[14]. However, in the situation where a subject moves, the waveform of a heartbeat might change over time due to body movements, which results in the degradation of the HR estimation accuracy.

In contrast, the direct RRI estimation methods estimate the RRI without the HR estimation by extracting each heartbeat component from the received signal of a Doppler sensor. The direct RRI estimation methods can be further classified into (i) the template matching-based one [15]–[17] and (ii) the feature-based one [18]–[22]. The template matching-based methods prepare a template waveform of a heartbeat in advance and then detect heartbeats by comparing the received signal with the prepared template waveform [15]–[17]. However, the waveform of a heartbeat might change over time, which makes it difficult to prepare various ideal template waveforms. In the feature-based method, heartbeats are detected based on the features of the signal due to a heartbeat. Most of the conventional methods use a peak of the waveform as a feature [18], [19]. Sakamoto *et al.* [20] have proposed the feature-based correlation method by not only a peak but also extreme points and inflection points of the received signal. However, the SNR of the received signal which is a time-domain signal is highly susceptible of the range between a Doppler sensor and a target, and the waveform of the received signal is likely to be deformed depending on the range. In addition, the waveform might be deformed due to even slight body movements. Hu *et al.* [21] have proposed the method that estimates the RRI based on zero crossing of the time-domain signal obtained through various signal processing, e.g., WT and EEMD (Ensemble Empirical Mode Decomposition). EEMD can decompose the analyzed signal to some components called IMF (Intrinsic Mode Function). The conventional method [21] performs the signal reconstruction based on some IMFs. However, in the conventional method, selecting optimum IMFs used in the signal reconstruction over all IMFs is challenging. Furthermore, unlike the ECG-based RRI measurement, this method estimates the RRI by the zero crossing detection of the analyzed signal, which causes some errors. Also, the direct RRI estimation method based on continuous WT has been proposed [22]. This method estimates the RRI through two steps: (i) learning and (ii) test ones. In the learning step, the scale factor corresponding to the HR is estimated. In the test step, continuous WT with the selected

scale factor is applied to the analyzed signal, which results in the time-domain signal called the wavelet coefficient. The RRI is then estimated by the peak detection of the obtained wavelet coefficient. This method has achieved a better RRI estimation accuracy than the other existing methods in the situation where a subject moves. However, the estimation accuracy of the scale factor corresponding to the HR depends on the center frequency of the prototype signal. In addition, the waveform deformation of the analyzed signal due to body movements might degrade the estimation accuracy of the scale factor corresponding to the HR, which might result in the incorrect peak detection. As can be seen from the above discussion, it is necessary to develop a more accurate RRI estimation method so that the accurate RRI-based stress evaluation such as the LF/HF assessment can be performed.

III. PROPOSED METHOD

In this section, as the extended version of our previous feature-based direct RRI estimation method [23], we propose a Doppler sensor-based RRI estimation method by the accurate peak detection. In our method, the spectra that are related with heartbeats are integrated not within [0.5, 2] Hz but within the higher frequency range which is not related with respiration and slight body movements, since the spectrum distribution of respiration and slight body movements is also related with that of heartbeats, e.g., [0.5, 2] Hz, which may degrade the RRI estimation accuracy. Unlike our previous method, the peaks due to heartbeats are detected using some peaks before and after the investigated peak so that the peaks due to non-heartbeats are not detected. In what follows, we explain the algorithm of the proposed method.

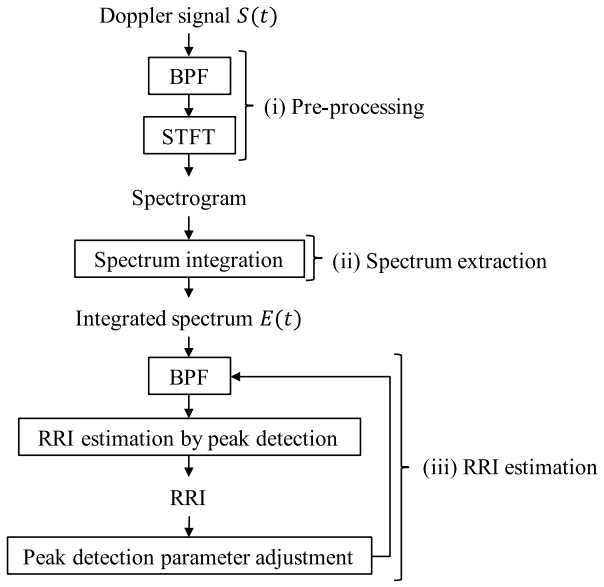

FIGURE 2. The flowchart of the proposed method.

Fig. 2 shows the flowchart of the proposed method. Our method mainly consists of three steps: (i) pre-processing, (ii) spectrum extraction, and (iii) RRI estimation. In the pre-processing step, BPF with the cut-off frequencies f_L and f_U is firstly applied to the Doppler signal $S(t)$ to roughly eliminate the frequency components of non-heartbeats, e.g., respiration and slight body movements. STFT with Hamming window is then applied to the filtered signal and a spectrogram is calculated. To extract the spectra due to heartbeats from the spectrogram, the time window used in STFT needs to be less than RRI so that it includes only one heartbeat. In our method, the time window and the overlap are set as 512 ms and 5 ms corresponding to 512 samples and 5 samples, respectively. Fig. 3 shows an example of in-phase and quadrature components, and Fig. 4 shows the spectrogram calculated from the in-phase and quadrature components shown in Fig. 3. From Fig. 4, it can be seen that the spectra due to heartbeats are distributed in both of the positive and negative frequency domains on the spectrogram. The spectrum in the positive frequency domain is associated with the heart diastole. In contrast, the spectrum in the negative frequency domain is associated with the heart systole. The frequency range is [8, 50] Hz and [−50, −8] Hz in the positive and negative frequency domains, respectively.

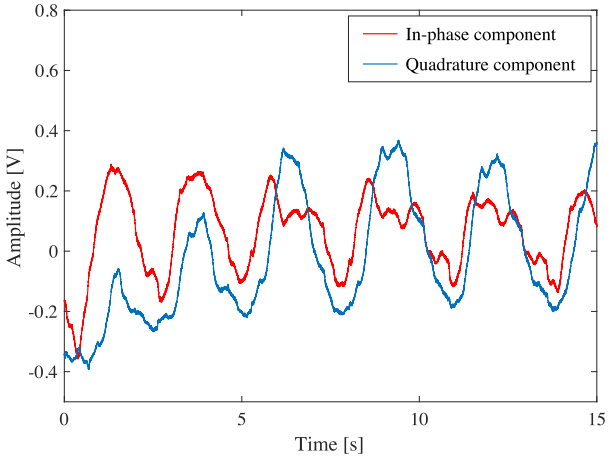

FIGURE 3. An example of in-phase and quadrature components.

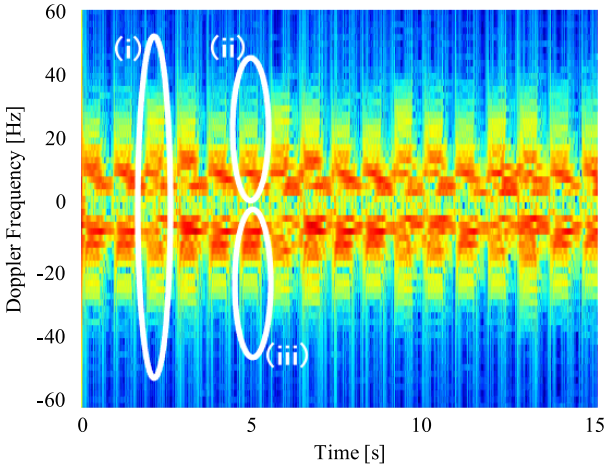

FIGURE 4. The spectrogram calculated from the filtered $S(t)$. (i) The spectrum due to a heartbeat. (ii) The spectrum associated with the heart diastole. (iii) The spectrum associated with the heart systole.

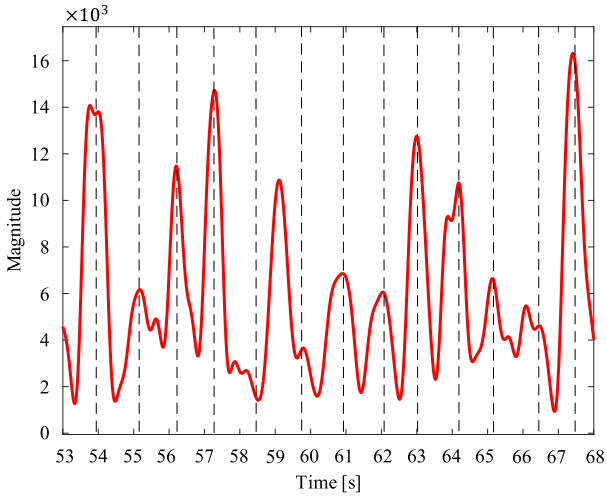

FIGURE 5. An example of the integrated spectrum. The dotted line denotes the actual timings of heartbeats.

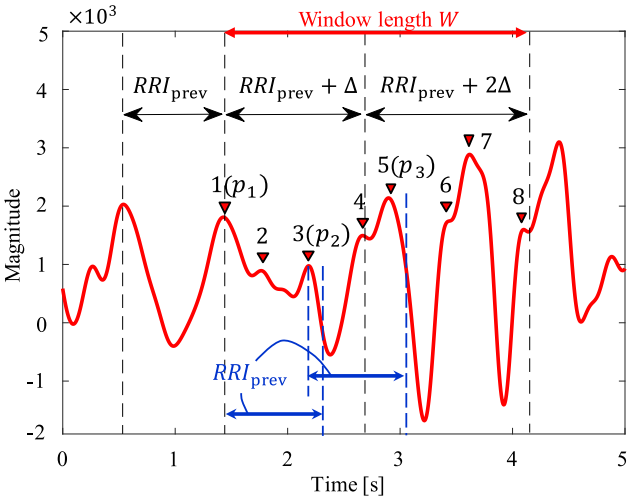

FIGURE 6. A concept of the proposed peak detection algorithm.

Based on this fact, the cut-off frequencies of BPF, f_{L} and f_{U}, are set as 8 Hz and 50 Hz, respectively, and these parameters are common for all subjects. In the second step, i.e., spectrum extraction step, the spectra within $[f_{\mathrm{L}}, f_{\mathrm{U}}]$ Hz and $[-f_{\mathrm{U}}, -f_{\mathrm{L}}]$ Hz are integrated. Fig. 5 shows the integrated spectrum. In this figure, the dotted lines denote the actual timings of heartbeats. In the RRI estimation step, the RRI is estimated by detecting the peaks of the integrated spectrum. However, the undesired peaks sometimes appear around the ones due to heartbeats as shown in Fig. 5. In our method, the peaks due to heartbeats are detected in what follows.

Algorithm 1 RRI Estimation Algorithm By the Peak Detection

Require: $p3 > p2 > p1$

Input: $Spec(t)$: the integrated spectrum

function RRI_estimator($Spec(t)$, W, $prevRRI$, f_{L2}, f_{U2})
  Apply BPF with its cut-off frequencies f_{L2} and f_{U2} to $spec(t)$
  Generate some pairs of the RRI candidates within the time window with its size W
  Find three peaks, $p1, p2$ and $p3$, so that the difference among two RRI candidates paired and RRI_{prev} is the smallest.
  Estimate RRI based on $p1$ and $p2$
  $prevRRI \Leftarrow RRI$
  PARAMETWR_TUNER(RRI_{prev}, Δ);
end function
function Parameter_tuner(RRI_{prev}, Δ)
  $W \Leftarrow 2RRI_{\mathrm{prev}} + 3\Delta$
  $overlap \Leftarrow RRI_{\mathrm{prev}}$
  $f_{\mathrm{L2}} \Leftarrow \frac{1}{RRI_{\mathrm{prev}}+\Delta}$
  $f_{\mathrm{U2}} \Leftarrow \frac{1}{RRI_{\mathrm{prev}}-\Delta}$
end function

Algorithm 1 shows the RRI estimation algorithm by the peak detection. In our peak detection, BPF is firstly applied to the integrated spectrum to reduce the effect of the undesired peaks. The way to set its cut-off frequencies f_{L2} and f_{U2} is explained later. After filtering, the peaks due to heartbeats are detected using some peaks before and after the investigated peak. Fig. 6 shows a concept of the proposed peak detection algorithm. In what follows, we explain how our peak detection algorithm works with this figure. Although eight peaks are observed in total within a time window in Fig. 6, some of them are related with heartbeats while others are due to noise. So it is necessary to choose only heartbeat peaks. Three peaks, p_1, p_2 and p_3 ($p_1 < p_2 < p_3$) are out of the peaks 1, 2, …, and 8 so that the difference among the previously estimated RRI RRI_{prev} and two pairs of RRI candidates is the smallest. This is because the RRI does not largely vary between the adjacent RRIs in general. Here, we denote $RRI_{i,j}$ as the RRI in between peaks i and j, where $1 \leq i \leq 8$ and $1 \leq j \leq 8$. In Fig. 6, assuming that RRI_{prev} is estimated correctly, the peak 1 is chosen as p_1. The pairs of $RRI_{1,k}$ ($2 < k < 8$) and $RRI_{k,m}$ ($k < m < 8$) are then generated, e.g., $RRI_{1,2}$ and $RRI_{2,5}$. As p_1, p_2 and p_3 that meet the condition where the difference among RRI_{prev}, $RRI_{1,k}$ and $RRI_{k,m}$ is the smallest, the peaks 1, 3, and 5 are finally chosen. Based on the fact that the RRI does not largely vary between the adjacent RRIs in general, a time window is set using the previously estimated RRI RRI_{prev}. Now, let Δ be the maximum difference between the current and previous RRI. When RRI increases by Δ twice in a row, the current RRI RRI_{curr} is equal to $RRI_{\mathrm{prev}} + \Delta$ and then the next RRI is equal to $RRI_{\mathrm{curr}} + \Delta$, i.e., $RRI_{\mathrm{prev}} + 2\Delta$ as shown in Fig. 6. Therefore, the length of a time window W is set as eq. (8) so that the window includes just three heartbeats.

$$W = 2RRI_{\mathrm{prev}} + 3\Delta, \tag{8}$$

where Δ is set as 150 ms in our method. In the initial observation where RRI_{prev} is not still estimated, the peaks due to heartbeats are detected by a simple peak detection for several seconds including two or three heartbeats. On the

other hand, when RRI decreases by Δ twice in a row, the time window calculated as eq. (6) includes three or four heartbeats depending on RRI_{prev}. For each window set in this way, only one RRI is estimated based on the peaks $pks1$ and $pks2$ in our method. RRI_{prev} is updated to the estimated RRI, i.e., $RRI_{1,3}$. The time window with the length W steps by RRI_{prev}. The overlap of a time window is then set as RRI_{prev}. Furthermore, since the maximum difference between the current and previous RRI is determined as Δ, the cut-off frequencies f_{L2} and f_{U2} are set using RRI_{prev} and Δ as eqs. (9) and (10), respectively, which results in the reduction of the number of the peaks due to non-heartbeats.

$$f_{\text{L2}} = \frac{1}{RRI_{\text{prev}} + \Delta}, \tag{9}$$

$$f_{\text{U2}} = \frac{1}{RRI_{\text{prev}} - \Delta}. \tag{10}$$

In the initial observation, f_{L2} and f_{U2} are initialized to be 0.5 Hz and 2 Hz corresponding to 30 bpm and 120 bpm, respectively.

IV. EXPERIMENTAL EVALUATION

To evaluate the performance of the proposed method, we conducted the experiments in three cases where a subject was (i) sitting still, (ii) typing, and (iii) speaking. We then compared the RRI estimation accuracy of our method with those of novel and state-of-the-art methods, i.e., the wavelet-based [22], the EEMD-based [21], and the MUSIC-based methods [10]. The wavelet-based method achieves a better RRI estimation accuracy than the other existing direct RRI estimation methods against a subject with body movements [22]. The EEMD-based method leverages the combination of some advanced signal processing techniques, e.g., the WT-based filter and EEMD [21]. This method has been shown to be accurate, and it is used for the LF/HF estimation as well as our proposed method. Also, the MUSIC-based method has been shown to be accurate even in the situation where a subject drives [10]. As the performance metric, the RSME between the estimated RRI and the ground truth value of the RRI is calculated as eq. (11).

$$RMSE = \sqrt{\frac{1}{N}\sum_{n=1}^{N} |RRI_{\text{est}}(t_n) - RRI_{\text{ref}}(t_n)|^2}, \tag{11}$$

where N denotes the number of the RRIs observed in one observation. t_n also denotes the time when the n th peak appears, and RRI_{est} and RRI_{ref} denote the estimated RRI and the ground truth value of the RRI, respectively. Furthermore, the stress index LF/HF is calculated based on the estimated RRIs. The LF/HF value can be calculated based on the spectrum analysis of the RRI variation [3], [4]. Specifically, the index is a ratio of the power spectrum density within the low frequency range, LF, to the one within the high frequency range, HF, where the low and the high frequency ranges are $[0.04, 0.15]$ Hz and $[0.15, 0.4]$ Hz, respectively. The LF reflects both sympathetic and parasympathetic activities, while the HF mainly reflects the parasympathetic activity. To evaluate the estimation accuracy of the LF/HF, the RE (Relative Error) between the estimated LF/HF and the ground truth value of the LF/HF is calculated as eq. (12).

$$RE = \frac{|x - r|}{r} \times 100, \tag{12}$$

where x and r denote the estimated LF/HF and the ground truth value of the LF/HF, respectively.

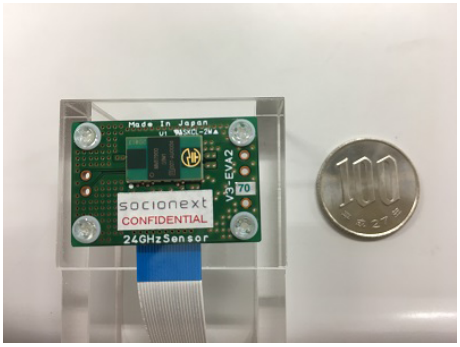

FIGURE 7. 24 GHz Doppler sensor.

TABLE 1. The specification of a Doppler sensor.

Item	Value
Modulation method	Unmodulated continuous wave
Carrier frequency	24 GHz
Sampling frequency	1,000 Hz
Transmission power	1 mW

Fig. 7 shows the Doppler sensor used in the experiments and the specification of the Doppler sensor is listed in TABLE 1. The carrier frequency and the transmission power of the Doppler sensor were 24 GHz and 1 mW, respectively, and the sampling frequency was set as 1000 Hz. The parameters used in the experiments are also listed in TABLE 2.

TABLE 2. The specification of the experiment.

Item	Value
Case	(i) sitting still, (ii) typing and (iii) speaking
Range d_0	80 cm in the case (i), 30 cm in the case (ii) and (iii)
Number of subjects	10
Observation duration	2 minutes
Number of observations	2 times for each case

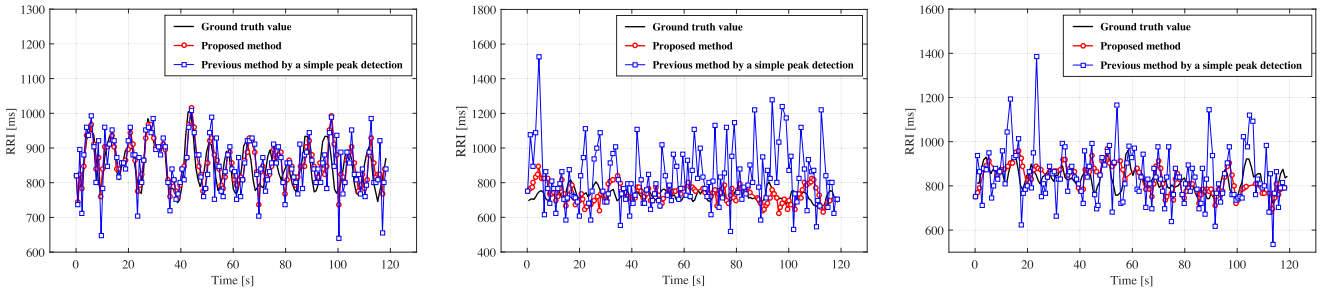

FIGURE 8. Examples of the RRI variation estimated by our proposed and previous methods in three cases of (i) sitting still, (ii) typing, and (iii) speaking.

In the experiments, the distance between the Doppler sensor and subject's chest, $d0$, was 80 cm in the case of sitting still and it was 30 cm in the other cases, i.e., typing and speaking. The observation was made on 10 subjects. The observation duration was 2 minutes for each case and the observation was repeated 2 times. The ground truth value of the RRI is calculated based on the data observed by ECG.

A. RRI ESTIMATION RESULT

The data of 10 subjects is listed in TABLE 3. Fig. 8 shows examples of the RRI variation estimated by our proposed and previous methods in three cases of (i) sitting still, (ii) typing, and (iii) speaking. Also, Fig. 9 shows an example of the RRIs estimated by our proposed method and the other existing methods, i.e., wavelet-based [22], EEMD-based [21], and MUSIC-based methods [10], in the case of sitting still. As can be seen from Fig. 8, our proposed method estimates the RRI more accurately than our previous one does. Furthermore, from Fig. 9, it can be seen that our method performs most accurate RRI estimation among all the methods. TABLE 4 shows the comparison of the average RMSE achieved by various RRI estimation methods. As a result, our proposed method outperforms the other existing methods [10], [21], [22] by the average RMSE in all the cases of sitting still, typing, and speaking. Also, our proposed method achieves the small RMSE, compared with our previous method. In particular, in the cases of typing and speaking, the estimation accuracy achieved by our previous method gets degraded compared with the one achieved by the proposed method. This is because more peaks due to body movements appear over the integrated spectrum in the cases of typing and speaking as shown in Fig 10, and then our previous method detects more peaks due to such non-heartbeats. In contrast, the proposed method reduces the number of the incorrect peak detection by detecting the peaks due to heartbeats based on some peaks before and after the investigated peak. As a result, our method improves the average RMSEs achieved by our previous one by 48.8 %,

TABLE 3. Data of 10 subjects.

Subject	Sex	Case	Actual average RRI [ms]
A	Male	Sitting still	950.9
		Typing	867.7
		Speaking	877.8
B	Male	Sitting still	845.7
		Typing	880.4
		Speaking	865.8
C	Male	Sitting still	857.8
		Typing	807.0
		Speaking	825.9
D	Male	Sitting still	769.2
		Typing	756.6
		Speaking	700.5
E	Female	Sitting still	658.3
		Typing	673.4
		Speaking	674.5
F	Female	Sitting still	828.2
		Typing	808.5
		Speaking	749.1
G	Male	Sitting still	828.2
		Typing	808.5
		Speaking	749.1
H	Male	Sitting still	828.2
		Typing	876.6
		Speaking	781.8
I	Male	Sitting still	744.4
		Typing	716.0
		Speaking	728.2
J	Male	Sitting still	929.5
		Typing	857.8
		Speaking	828.2

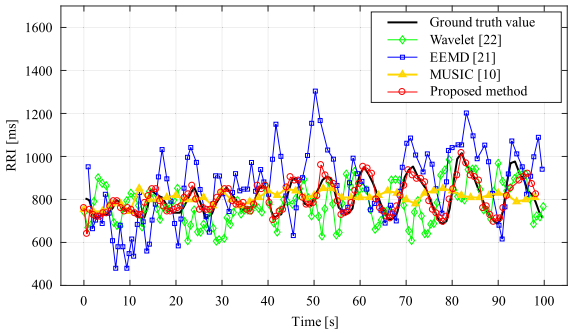

FIGURE 9. An example of the RRIs estimated by our proposed method and other existing methods in the case of sitting still.

TABLE 4. Comparison of the average RMSEs achieved by our proposed and other existing methods.

Case	Wavelet [22]	EEMD [21]	MUSIC [10]	Our previous method	Proposed method
Sitting still	122.8	131.4	93.2	92.6	47.5
Typing	168.8	183.3	91.5	137.7	78.9
Speaking	173.64	178.4	103.2	143.91	89.4

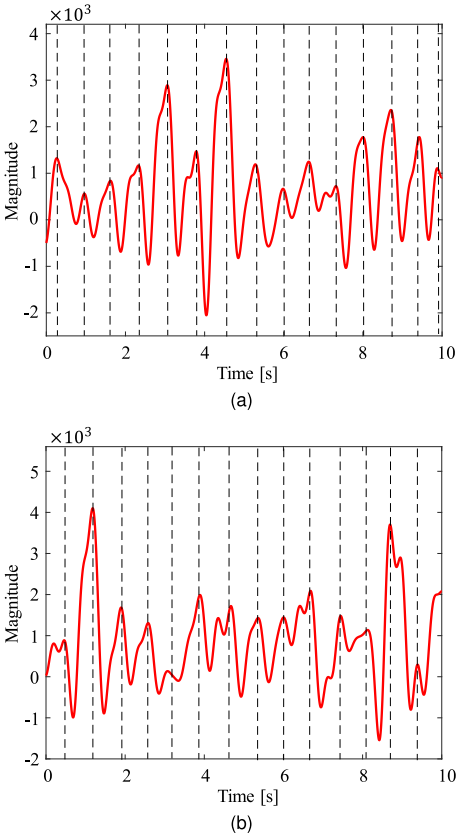

FIGURE 10. An example of the filtered integrated spectrum in the case of (i) sitting still and (ii) typing. The dotted line denotes the actual timings of heartbeats.

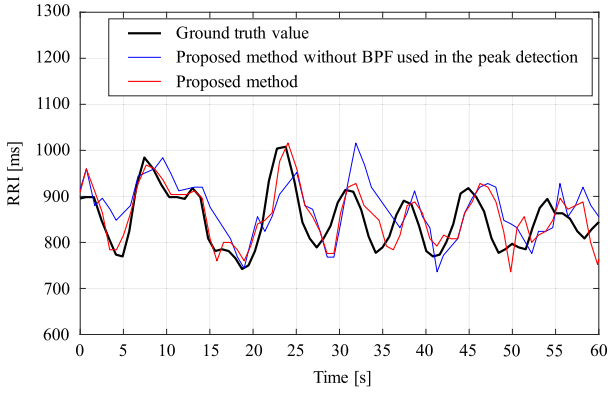

FIGURE 11. An example of the RRI variation estimated by the proposed method and the one without BPF used in the peak detection in the case of sitting still.

42.7 %, and 39.1 % in the cases of the sitting still, typing, and speaking, respectively. The reason why the RRI estimated by our method is not accurate completely is related with not only the noise due to respiration and slight body movements, but also the clutter and the interference in the background.

To better show the benefit of our proposed peak detection, we compare the proposed method with the one without BPF used in the peak detection. Fig. 11 shows the estimated RRI variation estimated by the proposed method and the one without BPF used in the peak detection in the case of sitting still As can be seen from this figure, our proposed method estimates the more accurate RRI than the one without BPF used in the peak detection does. As a result, our method improves the average RMSEs achieved by the one without BPF used in the peak detection by 14.3 %, 25.4 %, and 21.7 %, respectively. This is because the application of BPF with the cut-off frequencies determined based on the previously estimated RRI reduces the number of the peaks due to non-heartbeats.

B. LF/HF ESTIMATION RESULT

Figs. 12, 13, and 14 show examples of the LF/HF estimated by ECG, our previous and proposed methods in three cases of (i) sitting still, (ii) typing, and (iii) speaking, respectively. From these figures, it can be seen that our method estimates the LF/HF accurately, compared with our previous one does. Fig. 15 also shows the box plots for the REs of the LF/HF achieved by various RRI estimation methods. As can be seen from this figure, our proposed method outperforms the other methods by the average RE of the LF/HF in all the cases. This result is very positive to conclude that our method is superior to the state-of-the-art methods. Also, the experimental result shows that our method improves the average REs achieved by our previous one by 41 %, 53.9 %, and 14.2 % in the cases of sitting still, typing, and speaking, respectively. However, as can be seen from Fig. 15, the average REs achieved by our proposed method get degraded in the cases where a subject moves, i.e., typing and speaking, compared with the case of sitting still. This is mainly due to the degradation of the RMSE. To prevent the significant degradation of the LF/HF estimation accuracy, it might be better not to use the data that significantly degrades the RMSE in the real application.

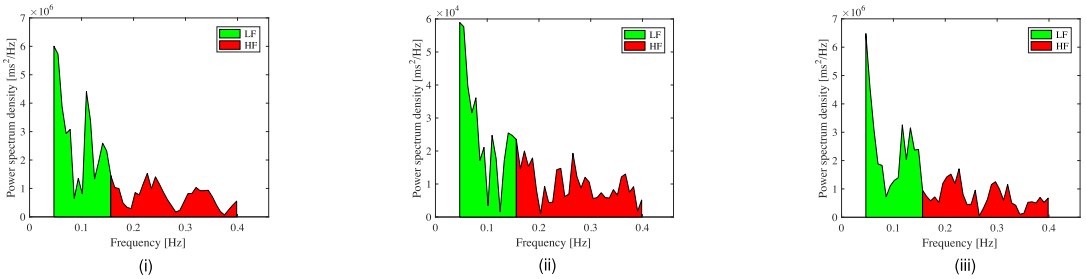

FIGURE 12. Examples of the LF/HF estimated by ECG, our previous and proposed methods in the case of sitting still.

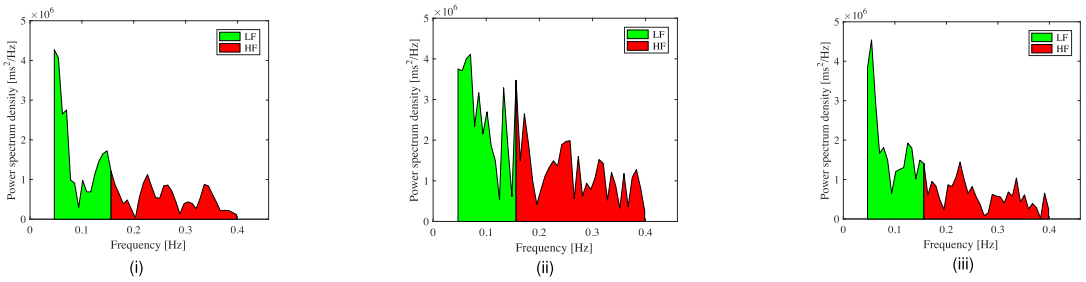

FIGURE 13. Examples of the LF/HF estimated by ECG, our previous and proposed methods in the case of typing.

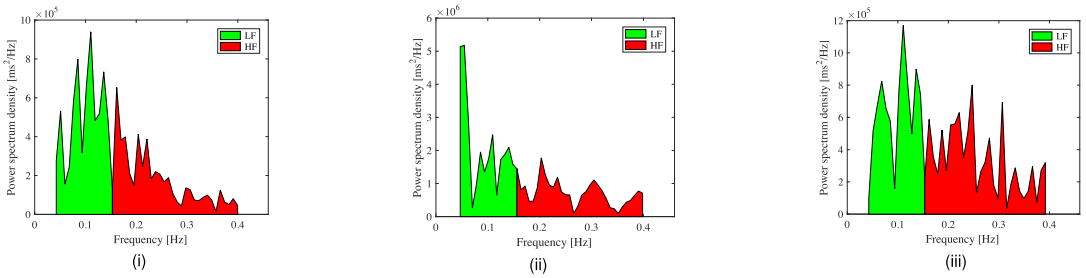

FIGURE 14. Examples of the LF/HF estimated by ECG, our previous and proposed methods in the case of speaking.

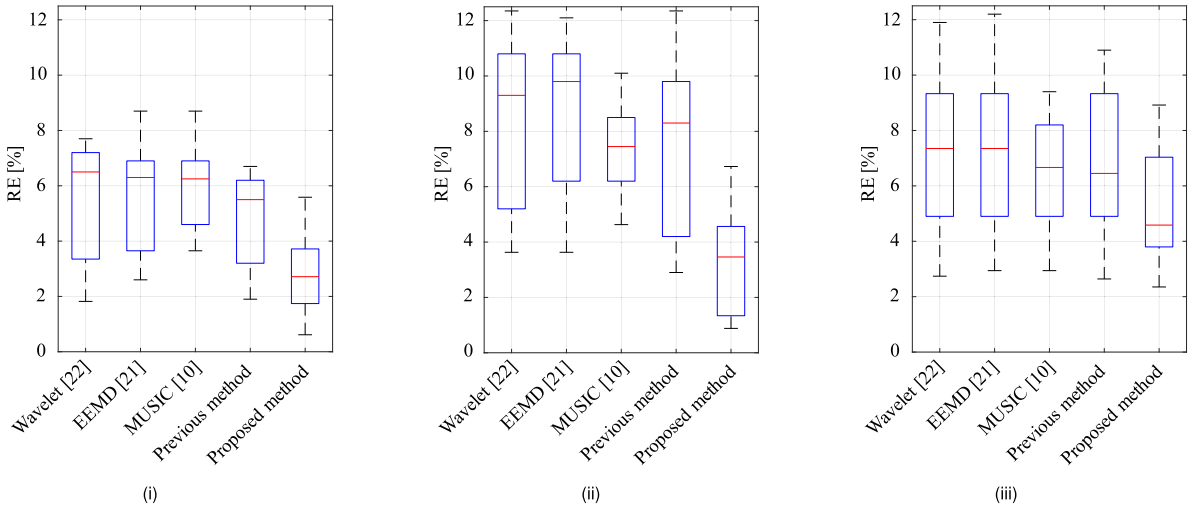

FIGURE 15. The box plots of the REs of the LF/HF achieved by our proposed and other existing methods in the cases of (i) sitting still, (ii) typing, and (iii) speaking.

V. CONCLUSION

In this paper, we proposed a Doppler sensor-based RRI estimation method by the accurate peak detection. In the proposed method, the spectra within the frequency range corresponding to heartbeats on a spectrogram are integrated. Some pairs of the RRI candidates are then generated based on the peaks within a time window, and three peaks are detected so that the difference among two RRI candidates

paired and the previously estimated RRI is the smallest. The time window length is updated over time based on the previously estimated RRI and the maximum difference between the current and previous RRI. We conducted the experiments on 10 subjects in the cases where a subject was sitting still, typing, and speaking. The experimental results showed that our proposed method outperformed the conventional and our previous ones by the RMSE and the estimation accuracy of the LF/HF. In particular, our proposed method improved the RMSE of our previous one by 48.8 %, 42.7 %, and 39.1 % in the cases of the sitting still, typing, and speaking, respectively. In our future work, for the sake of the accurate stress evaluation, it is necessary to develop the algorithm to detect the time when the RMSE of the estimated RRI significantly gets degraded.

REFERENCES

[1] M. Toichi, T. Sugiura, T. Murai, and A. Sengoku, "A new method of assessing cardiac autonomic function and its comparison with spectral analysis and coefficient of variation of R–R interval," *J. Auton. Nervous Syst.*, vol. 62, pp. 79–84, Jan. 1997.

[2] J. J. B. Allen, "Calculating metrics of cardiac chronotropy: A pragmatic overview," *Psychophysiology*, vol. 39, p. S18, Jan. 2002.

[3] M. Kumar, M. Weippert, R. Vilbrandt, S. Kreuzfeld, and R. Stoll, "Fuzzy evaluation of heart rate signals for mental stress assessment," *IEEE Trans. Fuzzy Syst.*, vol. 15, no. 5, pp. 791–808, Oct. 2007.

[4] A. Hernando *et al.*, "Inclusion of respiratory frequency information in heart rate variability analysis for stress assessment, *IEEE J. Biomed. Health Informat.*, vol. 20, no. 4, pp. 1016–1025, Jul. 2016.

[5] B. Lohman, O. Boric-Lubecke, V. M. Lubecke, P. W. Ong, and M. M. Sondhi, "A digital signal processor for Doppler radar sensing of vital signs," *IEEE Eng. Med. Biol. Mag.*, vol. 21, no. 5, pp. 161–164, Sep. 2002.

[6] G. Vinci *et al.*, "Six-port radar sensor for remote respiration rate and heartbeat vital-sign monitoring," *IEEE Trans. Microw. Theory Techn.*, vol. 61, no. 5, pp. 2093–2100, May 2013.

[7] C. Gu, G. Wang, Y. Li, T. Inoue, and C. Li, "A hybrid radar-camera sensing system with phase compensation for random body movement cancellation in Doppler vital sign detection," *IEEE Trans. Microw. Theory Techn.*, vol. 61, no. 12, pp. 4678–4688, Dec. 2013.

[8] J. Tu and J. Lin, "Fast acquisition of heart rate in noncontact vital sign Radar measurement using time-window-variation technique," *IEEE Trans. Instrum. Meas.*, vol. 65, no. 1, pp. 112–122, Jan. 2016.

[9] P. Bechet, R. Mitran, and M. Munteanu, "A non-contact method based on multiple signal classification algorithm to reduce the measurement time for accurately heart rate detection," *Rev. Sci. Instrum.*, vol. 84, p. 084707, Aug. 2013.

[10] K. J. Lee, C. Park, and B. Lee, "Tracking driver's heart rate by continuous-wave Doppler radar," in *Proc. Int. Conf. Eng. Med. Biol. Soc. (EMBC)*, Aug. 2016, pp. 5417–5420.

[11] A. Tariq and H. G. Shiraz, "Doppler radar vital signs monitoring using wavelet transform," in *Proc. Antennas Propag. Conf.*, Nov. 2010, pp. 293–296.

[12] A. Tariq and H. Ghafouri-Shiraz, "Vital signs detection using Doppler radar and continuous wavelet transform," in *Proc. 5th Eur. Conf. Antennas Propag. (EUCAP)*, Apr. 2011, pp. 285–288.

[13] M. Sekine and K. Maeno, "Non-contact heart rate detection using periodic variation in Doppler frequency," in *Proc. IEEE Sensors Appl. Symp.*, Feb. 2011, pp. 318–322.

[14] M. Li and J. Lin, "Wavelet-transform-based data-length-variation technique for fast heart rate detection using 5.8-GHz CW Doppler radar," *IEEE Trans. Microw. Theory Techn.*, vol. 66, no. 1, pp. 568–576, Jan. 2018.

[15] D. Nagaeand and A. Mase, "Measurement of heart rate variability and stress evaluation by using microwave reflectometric vital signal sensing," *Rev. Sci. Instrum.*, vol. 81, no. 9, p. 094301, 2010.

[16] S. Bakhtiari, S. Liao, T. W. Elmer, N. Gopalsami, and A. C. Raptis, "A real-time heart rate analysis for a remote millimeter wave I–Q sensor," *IEEE Trans. Biomed. Eng.*, vol. 58, no. 6, pp. 1839–1845, Jun. 2011.

[17] C. Will, K. Shi, R. Weigel, and A. Koelpin, "Advanced template matching algorithm for instantaneous heartbeat detection using continuous wave radar systems," in *Proc. Int. Microw. Bio Conf. (IMBIOC)*, May 2017, pp. 1–4.

[18] I. V. Mikhelson, P. Lee, S. Bakhtiari, T. W. Elmer, II, A. K. Katsaggelos, and A. V. Sahakian, "Noncontact millimeter-wave real-time detection and tracking of heart rate on an ambulatory subject," *IEEE Trans. Inf. Technol. Biomed.*, vol. 16, no. 5, pp. 927–934, Sep. 2012.

[19] T. Ohtsuki and E. Mogi, "Heartbeat detection with Doppler radar based on estimation of average R–R interval using Viterbi algorithm," in *Proc. IEEE Int. Symp. Pers. Indoor Mobile Radio Commun. (PIMRC)*, Aug./Sep. 2016, pp. 1–5.

[20] T. Sakamoto *et al.*, "Feature-based correlation and topological similarity for interbeat interval estimation using ultrawideband radar," *IEEE Trans. Biomed. Eng.*, vol. 63, no. 4, pp. 747–757, Apr. 2016.

[21] W. Hu, Z. Zhao, Y. Wang, H. Zhang, and F. Lin, "Noncontact accurate measurement of cardiopulmonary activity using a compact quadrature Doppler radar sensor," *IEEE Trans. Biomed. Eng.*, vol. 61, no. 3, pp. 725–735, Mar. 2014.

[22] E. Mogi and T. Ohtsuki, "Heartbeat detection with Doppler sensor using adaptive scale factor selection on learning," in *Proc. IEEE Int. Symp. Pers. Indoor Mobile Radio Commun.(PIMRC)*, Aug./Sep. 2015, pp. 2166–2170.

[23] E. Mogi and T. Ohtsuki, "Heartbeat detection with Doppler radar based on spectrogram," in *Proc. IEEE Int. Conf. Commun.*, May 2017, pp. 1–6.

[24] C. Gu, C. Li, J. Lin, J. Long, J. Huangfu, and L. Ran, "Instrument-based noncontact Doppler radar vital sign detection system using heterodyne digital quadrature demodulation architecture," *IEEE Trans. Instrum. Meas.*, vol. 59, no. 6, pp. 1580–1588, Jun. 2010.

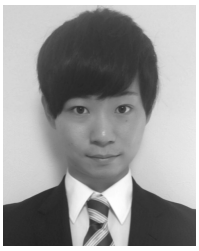

KOHEI YAMAMOTO (S'17) was born in Kanagawa, Japan, in1994. He received the B.E. degree from the Faculty of Science and Technology, Keio University, in 2017, where he is currently pursuing the master's degree with the Graduate School. His research interest is signal processing. He is a member of IEICE.

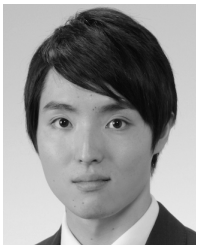

KENTAROH TOYODA (M'13) was born in Tokyo, Japan, in 1988. He received the B.E. M.E., and Ph.D. degrees in engineering from Keio University in 2011, 2013, and 2016, respectively. He is currently an Assistant Professor with Keio University. His research interest is security and privacy for systems and services with Internet of Things devices and financial technology. He received the Fujiwara Foundation Award in 2016, the Telecom System Technology Encouragement Award in 2015, and the IEICE Communication Society Encouragement Awards in 2012 and 2015, respectively. He is a member of IEICE and IPSJ.

TOMOAKI OHTSUKI (SM'01) received the B.E., M.E., and Ph.D. degrees in electrical engineering from Keio University, Yokohama, Japan, in 1990, 1992, and 1994, respectively. From 1994 to 1995, he was a Post-Doctoral Fellow and a Visiting Researcher in electrical engineering at Keio University. From 1993 to 1995, he was a Special Researcher of Fellowships of the Japan Society for the Promotion of Science for Japanese Junior Scientists. From 1995 to 2005, he was with the Science University of Tokyo. In 2005, he joined Keio University, where he is currently a Professor. From 1998 to 1999, he was with the Department of Electrical Engineering and Computer Sciences, University of California at Berkeley. He is involved in research on wireless communications, optical communications, signal processing, and information theory.

He was a recipient of the 1997 Inoue Research Award for Young Scientist, the 1997 Hiroshi Ando Memorial Young Engineering Award, the Ericsson Young Scientist Award 2000, the 2002 Funai Information and Science Award for Young Scientist, the 1st Asia-Pacific Young Researcher Award 2001 IEEE, the 5th International Communication Foundation Research Award, the 2011 IEEE SPCE Outstanding Service Award, the 27th TELECOM System Technology Award, the ETRI Journal's 2012 Best Reviewer Award, and the 9th International Conference on Communications and Networking in China 2014 Best Paper Award.

He has published more than 165 journal papers and 380 international conference papers. He is a fellow of the IEICE. He was the Vice President of the Communications Society of the IEICE, and he is the elected President of the Communications Society of the IEICE. He served as the Chair of the IEEE Communications Society, Signal Processing for Communications and Electronics Technical Committee. He has served the general-co chair and the symposium co-chair of many conferences, including IEEE GLOBECOM 2008, SPC, IEEE ICC2011, CTS, IEEE GCOM2012, SPC, and IEEE SPAWC. He served a Technical Editor of the *IEEE Wireless Communications Magazine* and an Editor of *Elsevier Physical Communications*. He is currently serving an Area Editor of the IEEE TRANSACTIONS ON VEHICULAR TECHNOLOGY and an Editor of the IEEE COMMUNICATIONS SURVEYS AND TUTORIALS. He gave tutorials and keynote speech at many international conferences, including IEEE VTC and IEEE PIMRC.